Chapter 4

COMPOUND PARABOLIC CONCENTRATOR FABRICATION AND CHARACTERIZATION

Given its potential for 50% module efficiency as described in [33], the winner of the Caltech Full Spectrum team's internal design competition and choice for full prototyping was the Polyhedral Specular Reflector (PSR). The simulated power conversion efficiency, though short of 50%, is higher than the state-of-the art as of this writing in 2016. This design uses seven distributed Bragg reflector (DBR) filters embedded at a 45° angle in a solid optical train as shown in Figure 3.2. Normally incident light enters the structure through a hollow, reflective primary compound parabolic concentrator. The primary concentration level is low to minimize the spread of angles hitting the filters for high optical efficiency of splitting. Each filter selectively reflects one band of light perpendicularly out of the incident beam into a receiver composed of a secondary concentrator and a subcell tuned to best convert that band of light. Parameters in the design include the overall size scale and the degree of primary, secondary, and overall concentration. Thus the name PSR refers not to a completely fixed design but a suite of designs that share the structure shown in 3.1e. The overall size scale and the degree of primary, secondary and overall concentration can be co-optimized for either $/W or high efficiency metrics. We opted to prototype a version of the PSR design optimized for highest efficiency. At the same time we explored the design space for a different version that would give the lowest cost. In order to prototype the highest efficiency design, we made and characterized compound parabolic concentrators (CPC) – the focus of this chapter. Explorations of the design's commercial potential are summarized in Chapter 5, including the cost model to design for lowest $/W.

4.1 Compound parabolic concentrator fabrication

Higher concentration improves efficiency (as described in Section 1.4) as long as the efficiency of concentration is high. Constraints on the level of achievable concentration in the PSR design include minimum cell edge length of about 1 mm. This is a rough lower bound for ease of manual handling during processing. Also, as the surface-area-to-volume ratio increases, surface recombination losses play more of a role, so for this reason we do not want smaller cells. In addition, we

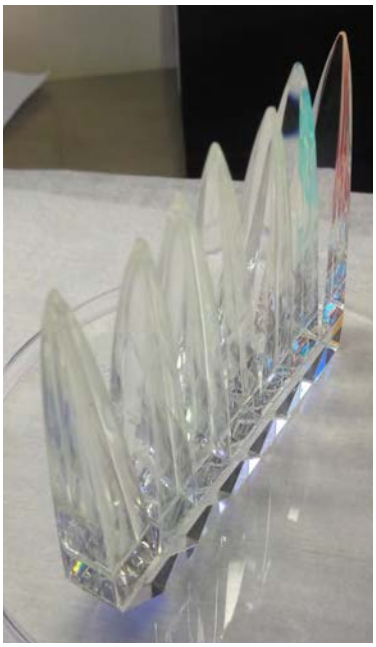

Figure 4.1: Schematic of the Generation IV Polyhedral Specular Reflector and photograph of PSR optical train with PDMS concentrators (images from Carissa Eisler).

restricted ourselves to an overall height of about 30 cm to avoid assembled modules being too heavy and unwieldy. A design with 1.73X primary concentration and 200X secondary concentrators was decided upon with highest possible module efficiency in mind. As intermediate steps toward this goal, we acquired or made a variety of compound parabolic concentrators (CPC). In total, we acquired and fabricated six different compound parabolic concentrator designs with distinct levels of concentration, material and cross-sectional shape to develop a measurement procedure and to understand trade-offs in efficiency.

CPC sources

We purchased a 13x Edmund Optics stock B270 glass circular cross-section CPC which was fire-polished after machining. Circular diamond-turned acrylic CPC were custom ordered from Syntec Optics at 15.6X and 27.7X. Finally, square injection molded CPC made of a proprietary plastic which was selected for visible light LED were also acquired from a vendor. Finally, Polydimethyl siloxane (PDMS) CPC with 77x and 194x concentration were fabricated in our labs. The lower concentration shape profile was milled into an aluminum block at the Caltech machine shop and then polished by hand using mechanical and chemical polishing. This piece was used to make molds in a low mechanical modulus PDMS (Sylgard 184 4:1 base:binder).

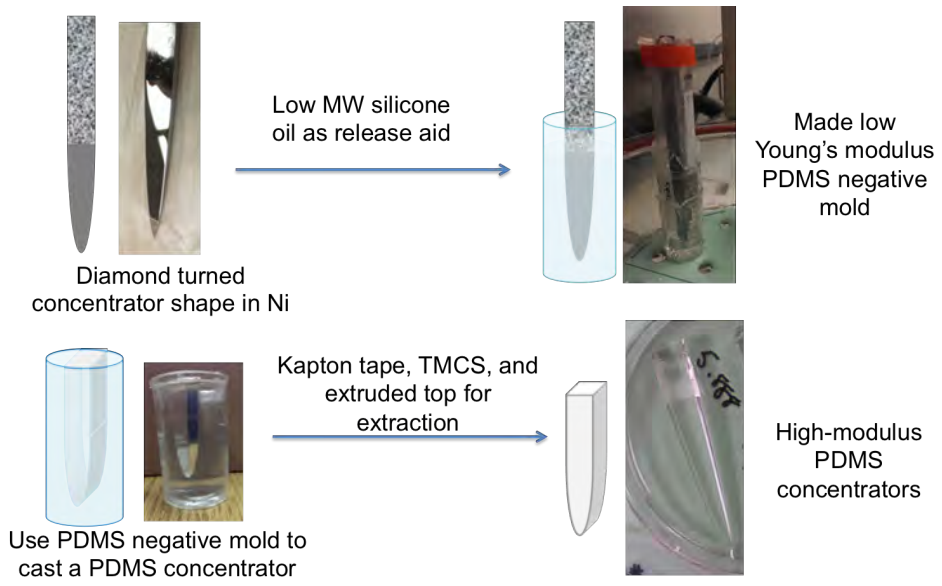

Figure 4.2: Schematic of the PDMS CPC molding process to make 194X concentrators using a high-quality diamond turned CPC form in a two-step molding process.

The mold was used to cast PDMS concentrators using a higher mechanical modulus PDMS mixture (Sylgard 184 2:1 base:binder). This process, shown schematically in Figure 4.2, was ultimately the most successful for producing CPC though yields remained low. For the higher concentration profile, Nipro Optics used single-point diamond turning to machine the square CPC profile into a thin layer of phosphorous alloyed Ni, plated on steel. The metal part was used to cast both electroformed molds by Nipro as well as PDMS molds in our lab to cast PDMS CPC.

The electroformed molds did not successfully produce usable CPC. The interior of the nickel mold surfaces had some imperfections that appeared to be particles stuck on the surface. These imperfections were transferred into molded CPC to the extent that they could be extracted. Attempts to extract crosslinked PDMS from the molds, however, invariably tore or otherwise damaged the concentrators. Having the PDMS stop flush with the top of the mold meant there was nothing to grab and use as leverage to pull the CPC out of the molds. PDMS is a very low surface energy material and the 194x CPC had a very large surface-area-to-volume ratio so a lot of friction needed to be overcome to extract the CPC from the molds. The PDMS was not compressible enough nor the mold large enough to fit grasping tools into the mold to exert pressure and grasp the CPC by two of its sides. In an attempt to overcome this challenge, we made tape collars at the top of the electroformed mold

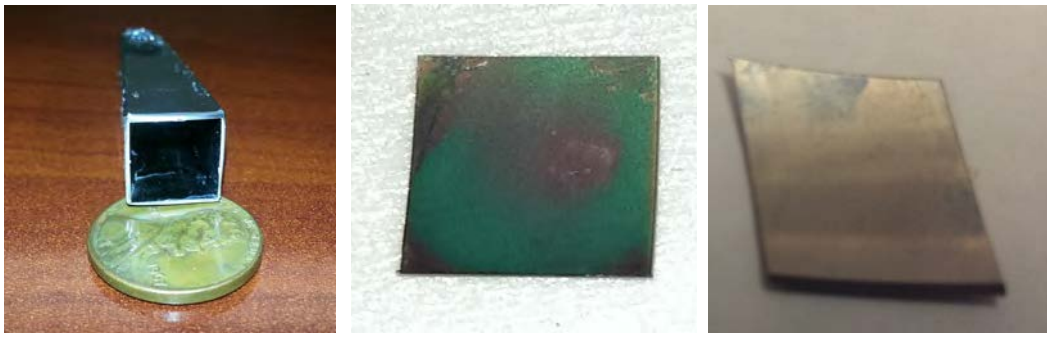

(a) Electroformed mold (b) Oxidized Ni (c) TMCS treated Ni

Figure 4.3: (a) Electroformed nickel mold with coin for scale showing some debris and scattering sources on the inside of the mold, (b) oxygen plasma cleaned nickel mold surface showing damage from oxidation, and (c) foggy nickel surface after exposure to trimethylsilyl chloride.

to create a knob on top that could be used to pull CPC up and out. However tears would often form in the PDMS at the height of the tape-mold interface. This likely occurred because the square CPC corner concentrated the stress applied. These tears would propagate tearing the whole CPC. In such cases, the PDMS in the mold would need to be cut into smaller extractable pieces. Cleaning the remaining PDMS out for reuse posed challenges. In a few cases this procedure worked to partially remove PDMS CPC from the electroformed molds if a tear formed lower in the structure. We could never successfully extract a whole CPC manually, however, so we investigated surface treatments and a non-manual extraction apparatus to facilitate extraction.

Various surface treatments were attempted on mostly flat test samples of a nickel electroform cut to about 1 cm by 1 cm by wire electric discharge machining (wire EDM). Motivated early on by the idea that the CPC were getting stuck on the visible surface imperfections of the molds, attempts to lubricate the PDMS-Ni interface started with improved cleaning of the nickel surface using both solvent rinsing and wiping with solvent moistened lens cloth. This did not change the ease of separation. Plasma cleaning nickel pieces caused oxidation of the surface leaving it roughened and damaged which a greenish tinge of nickel oxide. Trimethylsilyl chloride, a treatment often used on PDMS to modulate surface properties, left a foggy residue on the nickel surface that could be scratched off with wooden applicators or fingernails. PDMS curved against this foggy surface had this non-specularity transferred, resulting in rough rather than mirror-like PDMS molded surfaces. We additionally attempted to use low and high molecular weight silicone oil. The high molecular weight oil coated the mold with a macroscopically thick layer of oil that

ran during PDMS curing, leaving hundreds-of-micron to millimeter sized tracks in the molded CPC even after the oil treated mold was turned upside down and left to drip overnight. The low molecular weight silicone oil seemed to dissolve into PDMS, leaving no traces on the final part but also not improving ease of extraction. A visiting engineer who acted as a design consultant to this project designed a fixture for the bottom of the molds to attempt to blow pressurized air from the bottom of the mold to push the CPC out. However the opening at the bottom was $< 1mm^2$ in area. The first and only implementation of this concept did not exert enough force to remove parts from the mold.

CPC Measurement

For measurement, the PDMS CPC were cut on top using a razor blade to obtain a flat surface at the appropriate height. They were then attached using an optical adhesive to a glass cover slip to use as a handle and to provide a flat top interface. The top of the glass slide was taped off to make an aperture (Figure 4.4b,4.4c) with matte black tape. The circular cross-section Syntec CPC were epoxied into a collar at the top (Figure 4.4d), which reduced their effective aperture area from 9 mm diameter to 7.9 mm diameter without any additional interface between the CPC and light source. Finally square injection molded CPC also acquired from a vendor were held for measurement using a clamp to hold two parallel sides during measurement, so no additional interface was added nor was clear aperture lost.

Measurements were made using a large area, ABET solar simulator with divergence angle 1.3° as the light source. Two Advanced Photonix Si photodiodes were used to measure intensity at the input and output of the CPC, so these efficiency results are for the spectrum below ~1100 nm. Measurements were made using a solar simulator with an angle spread of 1.3° (half-angle of divergence). The reference photodiode was placed in the plane of the input face of the CPC as close to the input as possible (about 1 cm away) and the measurement photodiode was aligned with the bottom of the CPC to obtain the light intensity at the output of the CPC. Figure 4.5 shows photos of the setup from two angles including the measurement photodiode aligned with the output of a CPC and the reference photodiode mounted on the fixed platform used to hold the CPC. An x,y,z-stage setup was used for alignment and Cargille Refractive Index Liquids was used to form good optical contact between the CPC output and the top of the measurement photodiode.

As the measurement photodiode was raised from a position x-y aligned but far below

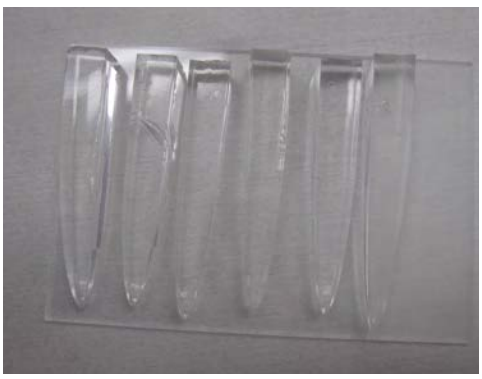

(a) 194X PDMS CPC

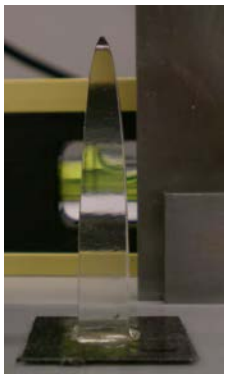

(b) 194X mounted

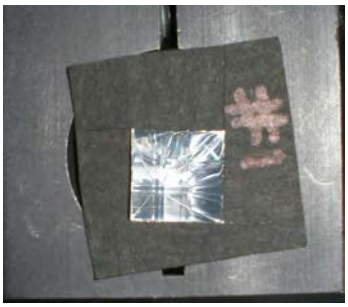

(c) 194X apertured

(d) Mounted circular CPC

Figure 4.4: CPC, fabricated and mounted for measurements, (a) Light being split in a partial optical prototype with the light path clearly visible due to scattering within the PDMS, (b) Series of PDMS cast CPC showing varying height and degrees of surface roughness, (c,d) Two views of a square PDMS CPC mounted to a glass coverslip with optical adhesive and apertured with black masking tape and (e) circular CPC mounted in a collar for efficiency measurements.

the CPC to close to the output face, the current increased slowly. The current jumped up when the index matching liquid on the photodiode came into contact with the tip of the CPC. Once in contact, I adjusted the stages to maximize the photodiode photocurrent. In some cases, this occurred when the photodiode was raised to the point that it pushed the whole CPC upward or when the CPC and photodiode were in sufficient mechanical contact that the motion of the photodiode in the x-y plane deflected the CPC tip. In these cases, it seemed that the deformation or displacement from force applied by contact with the photodiode was compensating for imperfections such as the top of the CPC being cut at a non-perpendicular angle to its axis or shape deformation of the tip. While this allowed slightly higher efficiency at the individual CPC measurement stage, it was a source of concern for a fully assembled device in which it would be preferable to have a CPC that provided the desired concentration well without needed to be strained in a particular

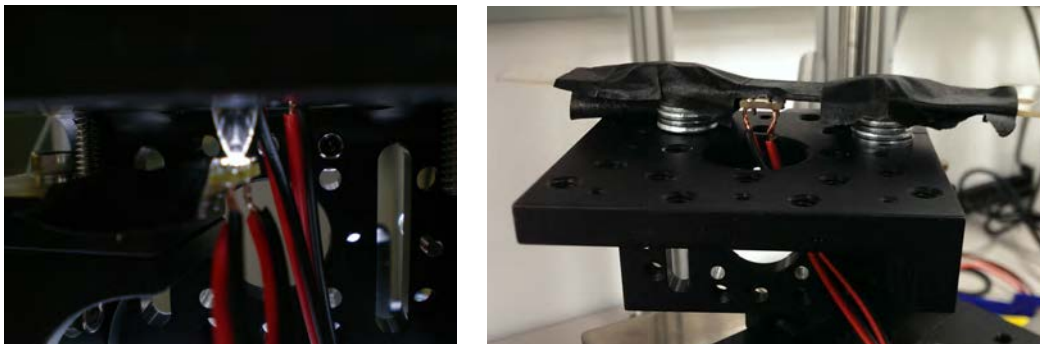

Figure 4.5: Measurement setup for CPC showing (left) the measurement photodiode attached to an x,y,z-stage setup for alignment and (right) the top photodiode mounted to a fixture that also holds the CPC in a fixed location. The top CPC setup was fixed in a location and the measurement photodiode was aligned with its output aperture to maximize the measurement photodiode current.

direction. The surface adhesion that posed challenges for mold extraction also caused problems at the cutting stage when the razor blade surface would stick and then suddenly release as more and more pressure was applied leading to uneven cuts. This made an internal interface that could scatter.

Our visiting engineer, Dirk-Jan Spaanderman, improved upon the manual cutting procedure by designing a jig to hold the CPC at 45° and the razor blade on a cutting track to even the pressure and the angle of the blade to remove some of the manual variability from cutting the CPC top. By initiating the cut at a corner with a smaller area of contact, less pressure was needed and thus less deformation induced in the whole CPC. Despite searching for a more effective cutting tool including the thinnest available gauge wire, individual steel wool threads, and a scalpel, no candidates were identified that could cut through PDMS more easily than a razor blade. While the jig improved cuts, the underlying problem of PDMS deforming as it was stressed and then suddenly slipping and creating a jagged edge along the input face persisted.

The efficiency of the CPC as measured in this setup is defined as

$$\eta = \frac{Output\ light}{Input\ light} = \frac{I_{mmt} * PDCF}{I_{ref} * \frac{A_{in}}{A_{PD}}}, \tag{4.1}$$

where I_{mmt} is the current of the measurement photodiode, I_{ref} the current of the reference photodiode, A_{in} input area of the CPC, and A_{PD} the area of the photodiode. The photodiode correction factor $PDCF$ was obtained by measuring the reference and measurement photodiodes against one another six times before each measurement to get the photodiode correction factor – the ratio of their currents

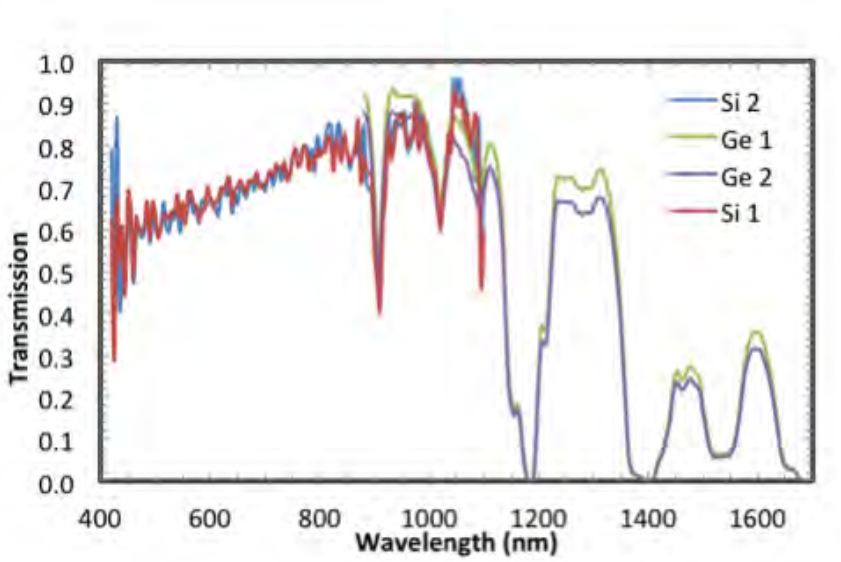

Figure 4.6: CPC transmission measurement using a supercontinuum laser source with monochromator and Si and Ge photodiode detectors showing large deviations from ideal transmission across all wavelengths and especially in the infrared.

from measurements at the same location. It is assumed that the spatial output of the source lamp is uniform so that the current can be scaled up by the ratio of areas of the CPC input face to the active area of the photodiode to obtain the light intensity hitting the CPC input. It is also assumed that no stray light is hitting the measurement photodiode; i.e., only light that is coming through the CPC output face hits the photodiode. Anecdotally, there is a shadow cast around the output of the CPC where light is totally internally reflected to the CPC output.

A second measurement setup was used to measure the best 194X PDMS concentrator. The source was a supercontinuum laser with a monochromater allowing spectrally resolved measurements. Additionally, both Si and Ge photodiodes were used to measure through 1700 nm.

CPC Results

The PDMS CPC made in our labs have some visible surface roughness and volume scattering. This can be seen especially well in Figure 3.2c in which a laser beam's path through the CPC is clearly visible. Table 4.1 summarizes the results of the measurements. First, Equation 4.1 was used to produce a raw efficiency. The best efficiencies of 194X CPC was 69.6%±3.1% and overall 77.6%±1% for 15.6X circular CPC where errors include only precision of the measurements. 4.2 summarizes relevant information on these five CPC shapes.

Samples				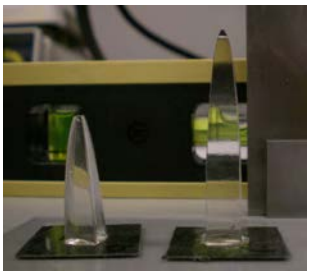	
Fabrication Method	Single-point diamond turning	Single-point diamond turning	Injection molding	cast from CNC machined positive	cast from diamond turned positive
Material	Acrylic	Acrylic	Proprietary plastic	PDMS	PDMS
Concentration	15.6X	27.7X	42.25X	77X	194X
Cross-sectional shape	Circle	Circle	Square	Square	Square
Output angle of CPC (°)	90°	90°	90°	50°	26°
Best Raw Efficiency	92%±2%	77.6%±0.7%	67.7%±0.8%	74.8%±1.3%	69.6%±3.1%
Preliminary corrected Efficiency	n/a	80% ±1%	70% ±1%	n/a	n/a

Table 4.1: CPC measurement Fresnel corrections

Preliminary corrections were made to the raw measured efficiency in order to back out the efficiency of the CPC itself by using ray tracing simulations. We sought to know the efficiency of the CPC itself (η_{CPC}) independent of its environment in order to appropriately use CPC measurements to estimate the efficiency of the whole photovoltaic module. This was done by assuming that the photodiode had only a 160 μm thick encapsulant layer (of refractive index $n = 1.42$ or $n = 1.59$, the lower and higher bounds for a clear plastic layer since the encapsulant material is unknown) on top of bare Si. A ray trace was done by my colleague John Lloyd for the photodiode in which a light source outputting isotropically into a half angle of 1.3° is incident on it. Fresnel reflections at the air-encapsulant interface and and the encapsulant-Si interface are the only loss mechanisms accounted for. The encapsulant is assumed to be lossless and the Si perfectly absorbing. The percent of incident light absorbed is found to be 74.8% with a low refractive index encapsulant or 77.3% if the encapsulant were high refractive index. Table 4.1 summarizes these

	77X PDMS CPC	42.2X Acrylic CPC	Photodiode alone
n = 1.42	75.1%	71.9%	74.8%
n = 1.59	78.2%	78.5%	77.3%
n = 1.42 correction factor	0.996	1.040	xx
n = 1.59 correction factor	1.029	0.985	xx

Table 4.2: CPC measurement Fresnel corrections

numbers for each combination. A second ray trace was done for the 27.7x acrylic circular CPC and the 77x PDMS square CPC. For the former a constant refractive index of 1.49 was used. For the latter a 200 μm glass coverslide was included as an additional interface and PDMS refractive index from [34] data across a wavelength range of 400-850 nm was used. In both cases, the CPC was assumed to be in index-matched optical contact with the encapsulant on the photodiode.

In the ray trace with the CPC, incident light is still 1.3° in angle spread at the input to the CPC, but as it propagates through the CPC by total internal reflection off the sidewalls, the angular spread increases up to the output angle (90° for the circular 27.7X CPC and 50° for the square 77X CPC), increasing Fresnel reflections off the encapsulant-Si interface. The percent absorption in the Si with the CPC in place is found to be 76% = $\eta_{RayTrace,CPC}$. Thus to back out the efficiency of the CPC, we use

$$\eta_{CPC} = \frac{\eta_{RayTrace,Photodiode}}{\eta_{RayTrace,CPC}} * \eta_{Measurement}. \tag{4.2}$$

This ability of the photodiode to absorb light at higher angles is not part of the internal efficiency of the CPC. In our device, the cells have specially designed anti-reflection coatings to ensure that light within our narrow spectral bands will be transmitted with high efficiency into the underlying cells for the angle range to which they are exposed. For both ends of the range of encapsulant refractive index, $\eta_{measurement}$ is close to one and thus not a significant source of loss.

Another loss mechanism is absorption in the concentrator material. Based on the absorbance given in Figure 4.9 and estimated optical path length of light passing through the CPC, 11% of light above the silicon absorption edge is absorbed by the PDMS CPC. To track down more of the remainder, a repeated measurement was made on our 'SARP' set-up. Using the SARP setup the transmission efficiency of the CPC was found to be 70% rather than 62.2% ± 4.3%. The SARP detector is a 1

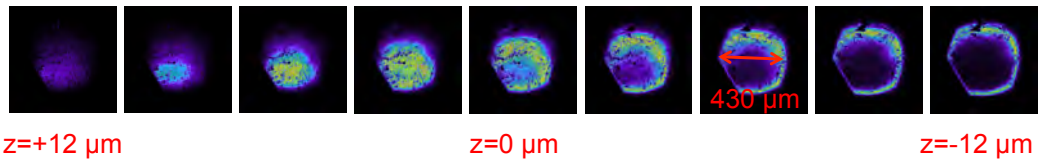

Figure 4.7: Confocal microscope image of the output face of the polished aluminum CPC showing significant rounding at the corners and bottom face itself on the order of tens of microns.

cm x 1 cm area versus 1.5 mm x 1.45 mm so scattering was through to play a role in this increased light collection.

Confocal microscope images of the tip of a CPC molded by the Al positive showed significant rounding of both the square cross-section and the outpout face (Figure 4.7). Ray tracking corner curvature suggests it causes some loss. Modeling the CPC shape with corner fillets of varying radius of curvature (between 1 μm and 300 μm shows a minor drop off for a single wavelength. As the fillet radius of curvature increases the effective acceptance angle (the angle within which CPC transmission efficiency is high) decreases.

CPC Discussion

The efficiencies of fabricated CPC are much lower than those of simulated concentrators. Potential losses could come from surface scattering, volume scattering, shape inaccuracy, absorption, and the attachment interface to the photodetector used in the characterization measurements. In addition to these, the PDMS CPC could have scattering at the top interfaces at the point of attachment to glass slides.

Generally, the circular cross-section CPC have higher performance than square cross-section CPC. First, circular cross-section CPC are more ideal than square cross-section CPC due to the absence of skew rays which can get bounced around the corners and ultimately rejected back out of the top of the structure rather than propagated to the output face. Additionally, the two circular cross-section structures have lower aspect ratios and were produced by single-point diamond turning. This precision fabrication method gives better surface quality and higher shape accuracy. The shape accuracy can diminish as the length and aspect ratio of the part increase, however. As the machine tool applies pressure to make cuts further from the anchoring point of the structure, more deflection will occur giving deviations from the intended curvature profile. Additionally, the 27.7X concentrator has a longer path length of plastic resulting in higher absorption losses. Between the two PDMS CPC,

similar arguments can be made for the 194X concentrator having higher absorption losses. The positive CPC at 194X was made by single-point diamond turning, a much more precision method, giving better surface quality than the CNC machined 77X positive. Its specular surface finish is shown in Figure 4.2. However the additional shape inaccuracy from the higher aspect ratio may or may not outweigh the benefit of moving the higher precision fabrication method. In fact the rougher surface might have allowed more scattered light to be collected by the photodiode in the measurement of the 77X concentrator providing another possible source of its higher efficiency. There are so many unknowns regarding the intended angle spread and material of the injection molded CPC that it is hard to draw many conclusions from its efficiency. It does however provide an existence proof demonstrating square CPC fabrication by molding.

Turning attention to the 194X CPC, the target of our efforts, in the visible and NIR portion of the spectrum measured by the silicon photodiode of the main measurement setup, absorption accounts for at least 10% of incident light lost. Due to the possibility of multiple reflections of skew rays, the total effective path length of light in the material is likely longer than the CPC height of 5.5 cm. Also a SARP measurement of a PDMS CPC with the output face obscured by mylar, so collecting light scattered light near the bottom of the CPC, showed about 5% of light collected. This leaves about 10-15% of losses unaccounted for.

The ray trace suggests that Fresnel reflections at the photodiode interface are not a significant source of variation in measurements of different CPC shapes. However the difference between measuring the rigid circular cross-section and molded CPC and the flexible PDMS CPC seems like it may cause differences. As described above, the flexibility posed problems both for repeatable CPC efficiency measurements and for obtaining the correct final shape due to difficulty cutting the top of the CPC to a flat surface. The aggregated results of this can be seen in Figure 4.1, where the photograph shows misalignment among the CPC relative to one another attached to the main filter train of the PSR. In this process we have realized that concentrators are not sufficiently produced parts to have good measurement standards. We developed characterization protocols with fixed angular spread sources and flat detectors. The full data that would have provided the internal efficiency of the CPC that we sought was transmission into a medium index matched to the CPC as a function of angle of incidence. We could have gotten full bidirectional scattering and/or reflectance distribution function by external characterization but this would only address surface

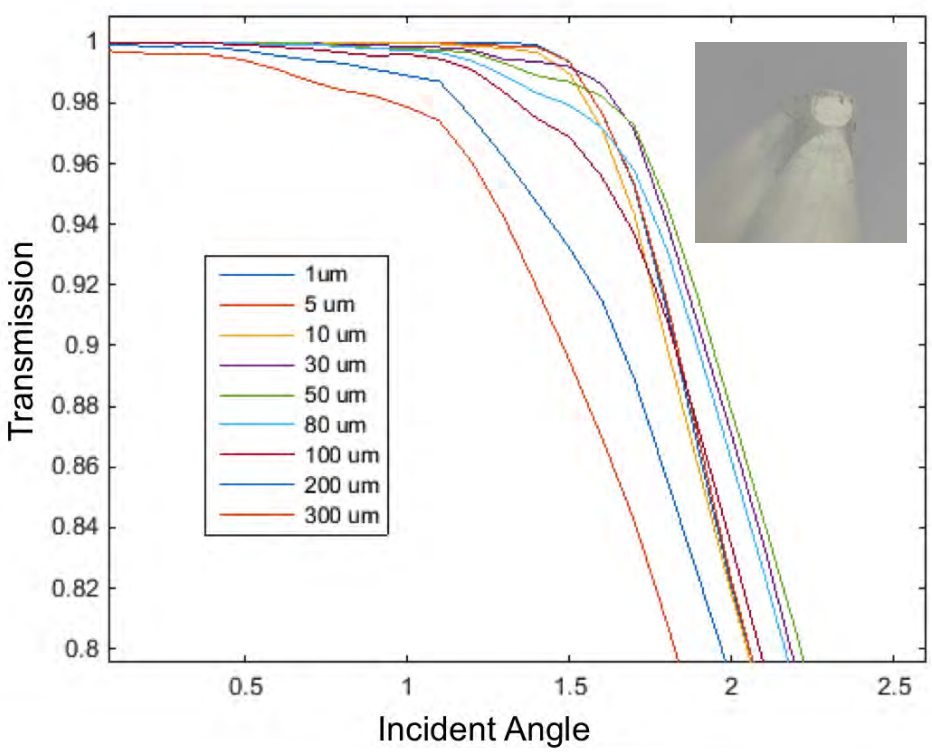

Figure 4.8: Ray trace simulation results for transmission efficiency of a CPC as a function of incidence angle with edge fillets of varying radius.

roughness by allowing us to incorporate the data into ray trace simulations.

We tested a couple of loss mitigation strategies. Toward the end of our time working on PDMS CPC, masters student Annabelle Sibue tried to mold the outer part of a CPC in PDMS around a glass piece. The goal was to have an embedded glass constitute most of the path length to avoid absorption losses. However extracting this heterogeneous structure from the molds without tearing the thin PDMS layers around the glass was more difficult than removing solid PDMS CPC. The thin layers tore very easily. Metal-coating the bottom sides on the CPC where light scatters out was a possibility, but the adhesion of thin metal layers to PDMS is poor and the specularity of a metal layer deposited on a rough surface would be low. We thought about improving the PDMS CPC quality by depositing a smoothing layer on the rough surface, but failed to find materials that could easier serve this role. Finally, a worthwhile experiment would have been measurement of incident light lost due to reflection back out the top of the CPC to determine the shape inaccuracy losses.

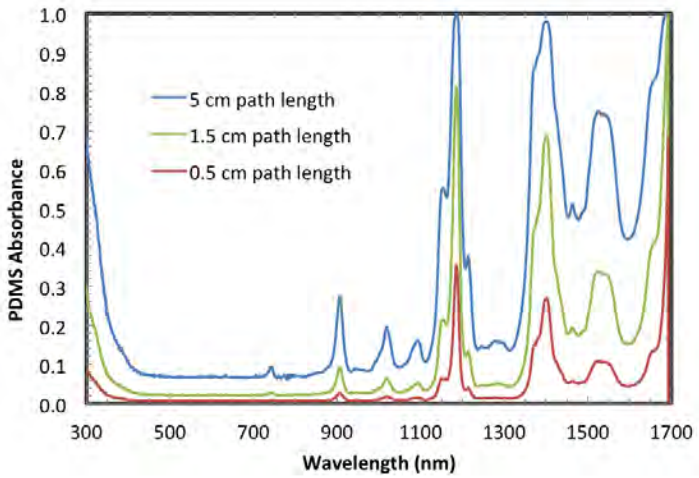

Figure 4.9: Sylgard 184 (2:1 base:curing agent) absorption as a function of path length calculated using measured extinction coefficient data.

Conclusion

We got to the point fabricating PDMS CPC at which we could repeatably mold ~70-75% efficiency 77X CPC and 65-70% efficient 194X CPC. This is far below the 95%-98% efficiency we saw in simulations and were banking on for an ultrahigh efficiency module. For the purpose of demonstrating a high-efficiency spectrum-splitting prototype, the decision was made to move to fused silica lightpipes which can be produced by coarse methods and then polished. We were able to find multiple vendors willing to give quotes for this type of part (unlike CPC), making them less of a struggle to acquire.

However, as discussed in the next chapter, moldable plastic optics are important for reaching high-volume, low-cost production. While PDMS is an optimal material for ease of lab-scale prototyping, the market for bespoke photovoltaic modules is quite small. Thus future work on commercially relevant concentrators should begin by exploring the trade-offs among plano-convex, Fresnel, lightpipe, and CPC concentrator designs with respect to efficiency and ease of fabrication in conjunction with experts in high-volume optics molding. At the academic scale the upfront cost for a mold is too high ($10-100k), especially if cycles of improvements are required for best quality results. On the other hand, even at the laboratory scale, polishing glass to roughness below $\frac{\lambda}{5}$ with an automatic polisher like the one in the Atwater labs is possible.

If there is reason to further explore how to make a high efficiency silicone concentrator, the first steps I would suggest would to be carefully determine our precision

Ni positive's shape profile by a metrology tool. A homemade version might use the deflection of a reflection laser spot to determine the curvature. A commercial example is something like Optical Gaging Products SmartScope ZIP 250. Secondly, I would determine the degree of corner rounding by careful microscopy. (It is a mistake to overlook the utility of optical microscopy or even a good camera's macro lens to assess if a part is as intended.) In the longer term, one would do well to redesign for a shorter path length of absorbing material (<1 cm). In order to ascertain what aspect ratio is feasible for mold removal, I would again use the Ni positive to cast molds of varying heights to attempt to identify if there is an aspect ratio below which removal is consistently possible. Finally, in order to avoid the cutting problem, the only solution I can see is to use sacrificial molds which include a top flat surface and a spout, in the spirit of an injection mold runner. The Ni positive could be used to cast a mold as usual. Then a microscope slide or some other flat surface could be adhered on to the top opening and a hole drilled into the side and a tube inserted that would be used to pour PDMS into the mold and ensure it did not empty out during degassing. The mold could then be cut off including the running portion. This would remove the cut from the critical top surface and place it on a side toward the top, which has much less of an implication for the overall optical efficiency.